ACS ES&T Engineering, Volume 6, Issue 4, April 2026, pp. 1285-1296
DOI: 10.1021/acsestengg.5c00994

Modeling Biofilm Growth on a CO_2-Supplying, Membrane-Based Biofilm Photobioreactor (MB-PBR)

J. Saul Garcia-Perez[a], Meenu Garg[a], Patricia Perez Calleja[a], Aura Ontiveros-Valencia[b], Roberto Parra-Saldivar[c], Robert Nerenberg[a*]

[a] Department of Civil and Environmental Engineering and Earth Sciences, University of Notre Dame, Notre Dame, Indiana, 46556, United States.

[b] División de Ciencias Ambientales, Instituto Potosino de Investigación Científica y Tecnológica, San Luis Potosí, 78216, México.

[c] Faculty of Engineering and Applied Sciences, Cranfield University, Cranfield, MK43 0AL, United Kingdom.

[*] Email: nerenberg.1@nd.edu

Abstract

The membrane-based photo biofilm reactor (MB-PBR) is a novel reactor that uses gas-permeable membranes to deliver carbon dioxide (CO_2) directly to the base of phototrophic biofilms. The CO_2 supply increases growth rates by reducing carbon limitation and pH increases, but the counter-gradient supply of CO_2 and light makes its behavior more complex. We developed a mathematical model to explore its behavior, and used a lab-scale MB-PBR to compare growth rates with and without CO_2 supply (control). After seven days, the MB-PBR biofilm grew to 186±10µm, compared to 101±10 µm for the control. The biomass productivity was 1.91±0.27 g/(m^2 d), compared to 0.49±0.06 g/(m^2 d) for the control. Using data fitting, the experimental light attenuation coefficient (k_e) and the half-saturation coefficient of light irradiance (K_I) were 80,000 1/m and 5 W/m^2, respectively. Modeling showed that, for a well-

Published by ACS. This is the Author Accepted Manuscript issued with: Creative Commons Attribution License (CC:BY 4.0).
The final published version (version of record) is available online at DOI:10.1021/acsestengg.5c00994. Please refer to any applicable publisher terms of use.

buffered system, increasing the CO_2 fraction in the gas supply increased the growth rate, but with diminishing returns: adding 5% CO_2 doubled the amount of growth, relative to the control, while adding 99% CO_2 only quadrupled the growth relative to the control. The beneficial effect of CO_2 supply was smaller for thicker biofilms and lower light intensities. With a weak buffer, CO_2 supply tended to acidify the biofilm interior, slowing growth rates at higher CO_2 concentrations. The model showed that, for the same light intensity and biofilm thickness, the maximum growth rate for the MB-PBR was higher, 0.141 g/(m^3 s), and was located closer to the CO_2 supply from the membrane. The conventional reactor had a maximum growth rate of 0.086 g/(m^3 s), located at the outer biofilm. The model is a practical tool that could be used, for example, to determine, for a given incident light intensity, water buffering, and CO_2 in the liquid and membrane supply, the optimal biofilm thickness at which to initiate harvesting. The model provides a fundamental understanding of membrane carbonated algal biofilms, as well as a tool to use the MB-PBR most effectively in practice.

Keywords: Membrane-biofilm photobioreactor (MB-PBR), CO_2 supply, counter-diffusion, microalgae, biofilm

1. INTRODUCTION

Phototrophic microorganisms, such as microalgae and cyanobacteria, are a promising resource for atmospheric CO_2 sequestration, wastewater treatment, and production of biofuels and high-value products such as antioxidants and pigments (e.g., phycocyanin, phycoerythrin, etc.) [1,2]. The engineered use of phototrophic organisms is based on photobioreactors, which may use planktonic growth or biofilm growth. While planktonic systems have historically been more common, biofilm photobioreactors have received increasing interest in recent years [3,4].

47 Advantages of biofilm photobioreactors include high cell densities, allowing for easier cell
48 collection [5], and smaller reactor footprints [6,7].
49
50 Carbon supply, pH control and O_2 inhibition are important considerations for all
51 photobioreactors, but especially for those based on biofilms. Carbon can become limiting in the
52 deeper biofilm, due to consumption and the mass transfer resistance, reducing overall growth
53 rates. While semi-immersed biofilm reactors receive continuous CO_2 supply from the air,
54 immersed photobioreactors often require supplemental bicarbonate or carbonate addition to the
55 bulk liquid [8]. Yet bicarbonate addition is often inefficient, as much of it is lost with the effluent.
56 Bubble diffusers can be used to deliver gaseous CO_2. However, these systems release CO_2 to the
57 atmosphere, as they have considerably low gas transfer efficiencies [9]. CO_2 can also be lost when
58 gas-permeable membranes are used to supply CO_2 to the bulk liquid [10–12].
59
60 Biofilm photobioreactors can pose additional challenges relative to suspended growth systems.
61 Phototrophic growth with nitrate or nitrite as the nitrogen source produces alkalinity, potentially
62 increasing pH beyond the optimum pH range of 6 to 9 [13]. The pH shifts can be accentuated in
63 biofilm systems, due to mass transfer resistance. Additionally, minerals can precipitate in the
64 biofilm at elevated pH, which may reduce growth rates and complicate biomass harvesting [14].
65
66 Another potential complication in biofilm systems is the accumulation of high levels of dissolved
67 O_2, a product of photosynthesis. O_2 competes with CO_2 for reduction at the RuBisCO enzyme,
68 and O_2 can become inhibitory at concentrations of around 1 mM (32 mg/L) [15]. Dissolved O_2 can
69 accumulate to high levels in thick biofilms exposed to high light intensities, due to O_2 production

in the deeper biofilm and the biofilm mass transfer resistance. An ideal photobioreactor reduces or avoids CO_2 limitation, O_2 inhibition, and pH inhibition. It supplies CO_2 while minimizing its loss with the effluent, and allows using CO_2 from waste sources.

The membrane-biofilm photobioreactor (MB-PBR), a novel photobioreactor based on gas-permeable membranes, provides many of the benefits described above. The membranes deliver CO_2 directly to the base of a phototrophic biofilm forming on the membrane outer surface. The supply of CO_2 directly to the biofilm interior allows up to 100% transfer efficiency, unlike conventional sparging systems, where gas is lost through bubbles escaping the bulk liquid [16]. It also minimizes CO_2 losses by precisely controlling gas pressure based on biofilm thickness. In addition, it can mitigate pH increases normally associated with phototrophic growth. It also can strip excess O_2 from the biofilm and can provide higher CO_2 concentrations at the base of the biofilm than conventional systems saturated with air.

Previous research has addressed photobioreactor configurations similar to the MB-PBR reactors. For example, Kumar et al. [9] studied *Spirulina* biofilms growing on a hollow fiber membrane photo-bioreactor based on CO_2-supplying hollow-fiber membranes. They studied biomass growth rates and CO_2 and nitrate removal efficiencies for different CO_2 concentrations in the gas phase. However, it appeared most of the algal growth was in the planktonic phase, not on the membranes. The membrane's relatively high packing density (200 m^2/m^3) likely limited growth directly on the membranes by restricting light penetration and limiting the available area for biofilm expansion. Bühler et al. [17] studied *Synechocystis* biofilms growing on a "segmented flow" capillary reactor, consisting of alternating liquid and gas segments, which enhances

performance by improving CO_2 mass transfer and providing hydrodynamic shear to stabilize biofilm thickness and prevent clogging. . They found the "segmented flow" reactor grew faster than the "single-phase" (conventional) biofilm. Li, et al [18,19] used experiments and modeling to explore the performance and behavior of a "porous substrate bioreactors" where the base of the biofilm was attached to a porous membrane exposed to liquid media, while the outer biofilm was exposed to air and light. Furthermore, Guo et al.[20] and Ding et al.[21] demonstrated the efficacy of gas-permeable membranes in enhancing CO_2 fixation and lipid productivity.

Modeling of biofilms on gas-permeable supports was pioneered by Semmens and Essila [22]. Most recently, researchers have modeled counter-diffusional biofilms and noted distinct behavior relative to conventional co-diffusional biofilms, e.g., Pérez-Calleja et al.; Wang et al.; Martin et al. 2013 [23–25]. Several studies have developed mathematical models for phototrophic processes, e.g., Aparicio et al. and Wolf et al. [26,27], as well as Liu and Liao [28], a work that focused on the practical aspects of optimizing CO_2 and nutrient fluxes in a carbonated membrane. The main novelty of our work is the development of a computational model of a photobioreactor with counter-diffusional supply of CO_2 and light. While others have previously published on CO_2-supplying photobioreactors, a model providing quantitative insights is lacking. We experimentally tested the MB-PBR and developed a biofilm model to explore its unique behavior, as compared to conventional phototrophic biofilms.

2. MATERIALS AND METHODS

2.1 Bench scale experiments

Mixed phototrophic inoculum.

The reactor inoculum was a mixed phototrophic culture collected from St. Joseph Lake in Notre Dame, Indiana, USA. A mixed culture was selected to ensure non-axenic conditions found in practical applications such as wastewater treatment and large-scale biomass production. Several mL of lake water was added to 500 mL of BG-11 [29] growth medium. The suspended culture was grown and maintained under semi-sterile conditions in BG-11 media [29] in a 500 mL bottle with constant mixing, aeration and continuous cold fluorescent LED light. The BG-11 media composition was 17.6 mM $NaNO_3$, 0.23 mM K_2HPO_4, 0.3 mM $MgSO_4 \cdot 7H_2O$, 0.24 mM $CaCl_2 \cdot 2H_2O$, 0.031 mM citric acid$\cdot 2H_2O$, 0.021 mM ferric ammonium citrate, 0.0027 mM $Na_2 \cdot EDTA \cdot 2H_2O$, 0.19 mM Na_2CO_3, 46 mM H_3BO_3, 9 mM $MnCl_2 \cdot 4H_2O$, 0.77 mM $ZnSO_4 \cdot 7H_2O$, 1.6 mM $Na_2MoO_4 \cdot 2H_2O$, 0.3 mM $CuSO_4 \cdot 5H_2O$, and 0.17 mM $Co(NO_3)_2 \cdot 6H_2O$.

Membrane biofilm photobioreactor (MB-PBR) configuration.

Two reactors were custom-built using clear acrylic rectangular flow cells with a 25-cm length and an internal square cross-section of 1.2x1.2 cm (**Figure 1**). The working volume of both reactors was 35 mL. Each flow cell had two ports at the bottom wall, where four silicone hollow-fiber membranes (Braintree Scientific, US) of 0.08 in (~2 mm) outer diameter and 0.04 in (~1 mm) inner diameter were inserted. On the top wall, there was a 2-cm long removable glass window to access the biofilm, although this was not removed in this research, and it was hermetically sealed with silicone and glue. The effective length of each membrane was 19 cm, measured as the length of the membrane that was suitable for biofilm growth in terms of light availability. In both the reactors, one end of the fiber was glued into a gas-supply manifold, which was connected to a gas tank using Norprene tubing (Cole Parmer, USA).

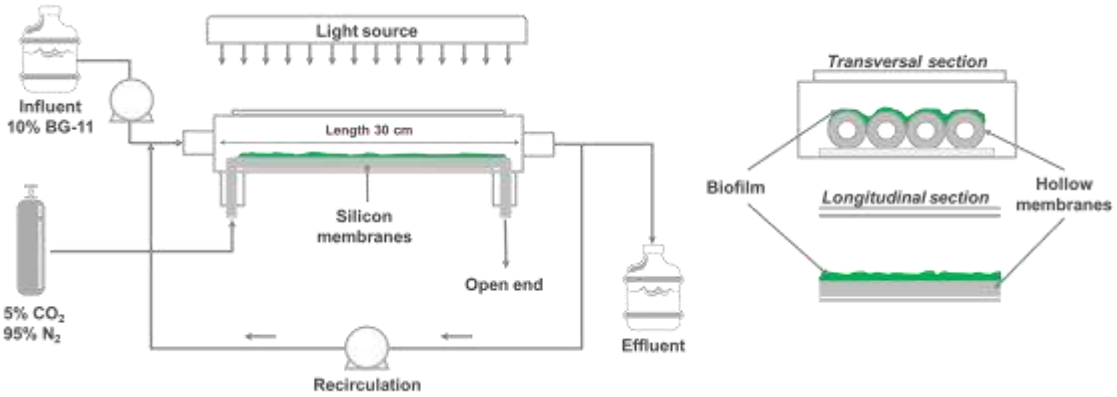

Figure 1. Experimental set up of MB-PBR. In the control, the membranes were closed.

Reactor 1 (MB-PBR) was supplied with a mixture of 5% CO_2 and 95% N_2 gases through the membrane in an open-end configuration [30]. Reactor 2 (control) had the membranes, but they were sealed at both ends.

Experimental set-up.

The reactor inoculum was prepared by growing a suspended phototrophic culture to exponential phase, then diluting it to achieve an optical density (OD_{750}) of 0.2-0.3. The reactors were filled with start-up medium and were operated in batch mode with recirculation (for mixing) to establish a biofilm on the membrane surfaces. Both reactors were maintained under well mixing by providing a high recirculation rate of 29 mL/min. One peristaltic pump (Masterflex L/S, Cole Parmer, USA) was used for recirculation. Upon inoculation, gases were supplied to the lumen of the fibers at 1 psi (6.9 kPa). The reactors were operated in batch mode for seven days before switching to continuous flow. A separate peristaltic pump (Rainin Dynamax RP-1, USA) provided influent to the reactors. The feed was prepared in a 20-L medium bottle under semi-sterile conditions. The continuous flow rate was 0.6 mL/min, providing an HRT of 58 minutes.

Both reactors were continuously illuminated by a cold white light LED screen (VT43WW3, Verilux, USA). The average light intensity at the top of the reactor was 85 μmol/(m^2 s).

The feed media for both reactors were exposed to atmospheric air, included bicarbonate (present in BG-11 media) and additional 16 mM phosphate buffer for pH control (pH was adjusted to 7.5). R1 (MB-PBR) was additionally supplied with 5% CO_2 through the hollow membranes, as described previously.

Biofilm imaging and biomass dry weight.

Biofilm images were collected periodically using optical coherence tomography (OCT) (Ganymede II Spectral Domain OCT System, THORLABS, Inc., Lübeck, Germany). OCT was used to obtain 2-D biofilm profiles since it is an *in-situ* and non-destructive imaging technique with high-resolution. The objective scan lens was a Thorlabs LSM03 with a center white light beam wavelength of 930 nm. It provided 4.1 μm axial resolution and 4.5 mm imaging depth in water. The image collection software was ThorImage OCT Version 4.3 (ThorLabs Inc.). The software settings included a 1.33 refractive index, 30 kHz image frequency, and 101 dB sensitivity.

The biofilm thickness was estimated as described by Lewandowski, et al (2007) [31]. Briefly, a MATLAB® script was used to convert OCT images to gray scale. Pixels were counted to quantify biofilm thickness.

The biofilm growing on the membranes was harvested by mechanical scraping, collected in pre-weighed 2.5 mL Eppendorf tubes with 1 mL of deionized water. The collected biomass was harvested by centrifugation (4,500 rpm, 10 min) and the dry weight was measured after 2 h at

T=105°C. Biomass productivities were calculated using a total surface area (scraping area) of 7.11×10^{-4} m^2.

2.2 Parameter estimation

Reported values of the light attenuation coefficient (k_e) and the half-saturation coefficient of light irradiance (K_I) within the biofilm are highly variable, and our model was very sensitive to these parameters (see **Table S4**). Therefore, we used two data sets to determine them by least squares minimization. Eight combinations of k_e (1/m) and K_I (W/m^2) were used to simulate the biofilm thickness over time and compared to the experimental values. The experimental values for biofilm thickness were averaged over three independent runs for both the membrane biofilm photobioreactor (MB-PBR) and the control reactor. The least-squares values, determined by minimizing the squared differences between experimental and model data, resulted in k_e=80,000 1/m and K_I=5 W/m^2. We used a third set of data to validate the calibrated model.

2.3 Model description

Two models for phototrophic biofilms were used for this study. One was a MB-PBR configuration, and the other a "control" conventional reactor, without CO_2 supply from the base of the biofilm. **Figure 2** provides a schematic representation of the model.

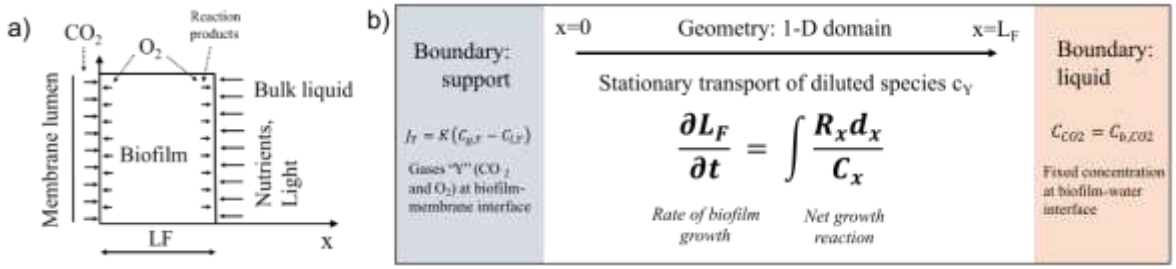

Figure 2. Schematic representation of the MB-PBR biofilm including (a) the physical biofilm structure with CO_2 coming from the membrane lumen and nutrients from bulk liquid and (b) the computational geometry, boundary conditions, and governing equations. J_Y=Mass flux of species "Y"; K=membrane mass transfer coefficient (for the control model, K was set to zero); C_Y=concentration of species "Y"; L_F=biofilm thickness; R_x=total reaction rate, C_x=Concentration of biomass; *x*=spatial coordinate for biofilm depth. Reaction products are the produced biomass and oxygen.

The kinetics and stoichiometry of phototrophic microbial processes were adapted from the PHOBIA photobioreactor model [27]. Key model features include: i) the supply of CO_2 from the hollow fiber membrane and bicarbonate from the bulk liquid (for the MB-PBR), or only from the bulk liquid as bicarbonate (for the control); ii) the growth of phototrophs utilizing either CO_2 or HCO_3^- as carbon sources, leading to an increase in biofilm thickness; iii) the computation of pH within the biofilm by considering proton production/consumption, speciation of carbonate and phosphate buffers; iv) the bidirectional diffusive transfer of CO_2 and O_2 through the membrane (in/out biofilm); (v) the exchange of solutes with the bulk liquid; (vi) diffusion of solutes in the biofilm; and (vii) the attenuation of light within the biofilm. The model outputs include the biofilm thickness over time, together with solutes concentrations, pH, light profiles and growth rates across the biofilm.

Model geometry

Both models assume a one-dimensional (1-D) biofilm (**Figure 2**) with properties varying only with biofilm depth (*x* direction). Planar geometry was assumed, neglecting the effect of hollow-fiber membrane curvature due to the thin biofilm.

State variables and constants

The state variables included concentrations of solutes: inorganic carbon species (CO_2, HCO_3^-, CO_3^{2-}), O_2, NO_3^-, water ions (H^+, OH^-), phosphate species ($H_2PO_4^-$, HPO_4^{2-}, PO_4^{3-}). The dissolved gases O_2 and CO_2 were transported by diffusion across the MB-PBR membrane and by diffusion through the biofilm, in both cases modeled using Fick's first law. The biomass was assumed to consist of phototrophs only, neglecting the potential presence of heterotrophic and nitrifying organisms. This was reasonable for our experimental system, as there was no organic matter or ammonium in the medium. Also, the short time between growth and harvesting likely minimized the secondary growth of heterotrophs on decay and soluble microbial products. A constant cell density C_x was assumed within the biofilm. Other inert particulate compounds, formed by decaying biomass, were neglected due to the short time scale (t=7 d) between experimental biofilm growth and harvesting.

Processes

Similar to Wolf et al. (2007) [27], the microbial processes included phototrophic growth on CO_2 (r_1) and on HCO_3^- (r_2), as well as endogenous aerobic respiration (decay) (r_3) . The stoichiometry of microbial processes is presented in **Table 1**, the process rates in **Table 2** and model parameters in **Table 3**. In order to explore the impact of light and oxygen inhibition on growth rates, some rate limitation factors were "turned off", as indicated in the Results and Discussion section.

Table 1. Stoichiometry of phototrophic growth and endogenous aerobic respiration. "S" denotes the concentration of a solute species.

	Solutes					Biomass	
Processes	S_H mol/m^3	S_{CO2} mol/m^3	S_{HCO3} mol/m^3	S_{O2} mol/m^3	S_{NO3} mol/m^3	C_x kg COD/m^3	Rate mol/(m^2 s)
Phototrophic growth on CO_2	$-Y_{NO3}$	$-Y_{CO2}$		1	$-Y_{NO3}$	Y_x	r_1
Phototrophic growth on HCO_3^-	$-Y_{NO3}$ - Y_{CO2}		$-Y_{CO2}$	1	$-Y_{NO3}$	Y_x	r_2
Endogenous aerobic respiration				-1			r_3

Table 2. Rates of phototrophic growth and respiration. Rates are expressed in moles of biomass per cubic meter per second (mol/m^{3}s), where one mole of biomass is defined by the empirical formula $C_{5.1}H_{8.5}O_{2.5}N$. Note that the COD equivalent is 1.34 kg COD/ kg biomass.

Rate mol/(m^3 s)	Rate expression
r_1	$q_{O2max,Ph}\left[\frac{S_{CO2}}{S_{CO2}+K_{s,CO2}\left(1+\frac{S_{O2}}{K_{I,O2}}\right)}\right]\left(\frac{S_{NO3}}{S_{NO3}+K_{s,NO3}}\right)\left(\frac{I}{I+K_I+\frac{I^2}{K_{LI}}}\right)\sigma_{low}(pH)C_x$
r_2	$q_{O2max,Ph}\left[\frac{S_{HCO3}}{S_{HCO3}+K_{s,HCO3}\left(1+\frac{S_{O2}}{K_{I,O2}}\right)}\right]\left(\frac{S_{NO3}}{S_{NO3}+K_{s,NO3}}\right)\left(\frac{I}{I+K_I+\frac{I^2}{K_{LI}}}\right)\sigma_{high}(pH)C_x$
r_3	$\beta_{resp}\left(\frac{S_{O2}}{K_{I,O2}+S_{O2}}\right)\left(\frac{K_I}{I+K_I}\right)C_x$

The rates (mol/(m^3 s)) depend on the availability of dissolved chemical compounds in concentrations S (mol/m^3) and light with intensity I (W/m^2), with various half-saturation coefficients K_s (mol/m^3), light saturation coefficients K_I, and maximum specific rates $q_{o2max,Ph}$ (mol/kg s) for growth and β_{resp} for endogenous respiration. Endogenous aerobic respiration, also known as phototrophic respiration, is the consumption of oxygen and organic matter in the absence of light. It's generally assumed to be about 10% of the maximum rate of oxygen production (β_{resp}=0.1$q_{O2max,Ph}$) [27]. The terms σ_{low}(pH) and σ_{high}(pH) are step functions

implemented in the model with a second order continuous smoothing at the beginning and end. The functions affect growth on CO_2 at pH values less than 5.5 and on HCO_3^- at pH values above 8.5, consistent with past research [32]. The availability of inorganic carbon species is determined by the carbonate system equilibrium, with pK_a values of pK_{a1}=6.35 and pK_{a2}=10.33 (**Table S2**). The uptake of specific carbon species is regulated by the step functions that account for physiological inhibition (**Figure S1**). The function σ_{low}(pH) regulates CO_2 uptake under acidic conditions; it transitions from 1 (full activity) to 0 (total inhibition) as pH drops from 5.0 to 4.0, reflecting acidic stress. Similarly, σ_{high}(pH) regulates HCO_3^- uptake under alkaline conditions, transitioning from 1 to 0 between pH 8.0 and 9.0 to account for inhibition at higher pH values where CO_3^{2-} begins to predominate and uptake of HCO_3^- is typically decreased.

The pH profiles were determined by modeling the acid-base equilibria of the carbonate and phosphate systems, as well as the dissociation of water (**Tables S2 and S3**). These reactions were implemented as reversible processes with a very fast but finite rate coefficient ($k_a=10^7$/s). This kinetic approach approximates instantaneous equilibrium. All chemical species in the system were assumed to have equal diffusion coefficients, allowing the pH computation via mass balance equations.

Light attenuation intensity within the biofilm was represented by the Beer-Lambert expression function of depth within the biofilm:

$$I(x) = I_0 e^{-k_e(L_F - x)} \qquad (1)$$

where "I" is the incident attenuated light (W/m^2) across the biofilm depth (x), "I_0" is the initial incident light (W/m^2), "k_e" is the light attenuation coefficient (1/m) and "L_F" is the biofilm thickness (m). The cell density was assumed constant throughout the biofilm, even in the deeper inactive zones. A light inhibition term (I^2/K_{LI}) was included in the microbial rates. The "k_e" was

279 estimated by fitting the model to experimental data. A conversion factor of 0.218 was used to
280 convert light units from µmol/m²/s to W/m^2 [33].

281

282 **Table 3.** Model parameters

Parameter	Symbol	Value	Units	Reference
Diffusion coefficients				
CO_2 diffusion coefficient in water at 20ºC	$D_{W,CO2}$	1.1×10^{-9}	m²/s	[34]
NO_3^- diffusion coefficient in water at 20ºC	$D_{W,NO3}$	1.72×10^{-9}	m²/s	[35]
O_2 diffusion coefficient in water at 20ºC	$D_{W,O2}$	2×10^{-9}	m²/s	[35]
N_2 diffusion coefficient in water at 20º C	$D_{W,N2}$	1.8×10^{-9}	m²/s	[36]
HCO_3^- diffusion coefficient in water at 20º C	$D_{W,HCO3}$	1.1×10^{-9}	m²/s	[34]
CO_3^{2-} diffusion coefficient in water at 20º C	$D_{W,CO3}$	1.1×10^{-9}	m²/s	[34]
$H_2PO_4^-$ diffusion coefficient in water at 20º C	$D_{W,H2PO4}$	1×10^{-9}	m²/s	[37]
HPO_4^{2-} diffusion coefficient in water at 20º C	$D_{W,HPO4}$	1×10^{-9}	m²/s	[37]
PO_4^{3-} diffusion coefficient in water at 20º C	$D_{W,PO4}$	1×10^{-9}	m²/s	[37]
H^+ diffusion coefficient in water at 20º C	$D_{W,H}$	8.42×10^{-9}	m²/s	[37]
OH^- diffusion coefficient in water at 20º C	$D_{W,OH}$	4.8×10^{-9}	m²/s	[37]
O_2 diffusion coefficient in membrane	$D_{m,CO2}$	3×10^{-9}	m²/s	[38]
CO_2 diffusion coefficient in membrane	$D_{m,O2}$	1.65×10^{-9}	m²/s	Calculated*
N_2 diffusion coefficient in membrane	$D_{m,N2}$	2.7×10^{-9}	m²/s	Calculated*
Equilibrium constants				
Henry coefficient O_2	H_{O2}	0.033	mol/mol	[40]
Henry coefficient CO_2	H_{CO2}	0.944	mol/mol	[40]
Henry coefficient N_2	H_{N2}	0.017	mol/mol	[40]
Kinetics and stoichiometry				
Maximum specific rate of oxygen production by phototrophs	$q_{O2max,Ph}$	8.58×10^{-4}	mol/(kg s)	[27]
Specific rate of oxygen consumption during phototrophic respiration (decay)	β_{resp}	8.58×10^{-5}	mol/(kg s)	[27]
CO_2 half saturation coefficient	$K_{s,CO2}$	0.1	mol/m³	[27]
HCO_3^- half saturation coefficient	$K_{s,HCO3}$	0.1	mol/m³	[27]
NO_3^- half saturation coefficient	$K_{s,NO3}$	0.0012	mol/m³	[27]
O_2 inhibition constant	$K_{I,O2}$	0.3	mol/m³	[27]
Yield for biomass	Y_x	0.023881	kg/mol	[27]
Yield for NO_3^-	Y_{NO3}	0.12687	mol/mol	[27]
Yield for CO_2	Y_{CO2}	0.74627	mol/mol	[27]
Half-saturation coefficient of light irradiance	K_I	5	W/m^2	Estimated

Density of biomass	C_X	20	kg COD/m³	Chosen
Light attenuation coefficients	k_e	80,000	1/m	Estimated
Light inhibition coefficient	K_{LI}	50	W/m^2	Chosen
Operational conditions				
Initial biofilm thickness	L_{F0}	3×10^{-5}	m	Experiment
Membrane thickness	d_m	5.08×10^{-4}	m	Experiment
Temperature	T	293.15	K	Experiment
*Bulk concentrations**				
Bulk nitrate concentration	$c_{i,NO3}$	1.76	mol/m³	10% BG-11 media
Bulk phosphate concentration in influent*	c_{i,P_T}	16.023	mol/m³	10% BG-11 media + buffer system
Bulk total inorganic carbon (Ci) concentration (in equilibrium with air)	$c_{i,CO2_T}$	0.035	mol/m³	Atmospheric CO_2 +10% BG-11 media (bicarbonate)
Influent pH	pH_i	7.5		Experiment
Light intensity at outer biofilm**	I_0	18.5	W/m^2	Experiment
Total gas pressure in membrane	p_{tot}	1.21×10^5	Pa	Experiment
Bulk O_2 concentration	$c_{i,O2}$	0.291	mol/m³	Chosen
Bulk N_2 concentration	$c_{i,N2}$	0.549	mol/m³	Chosen

* Derived from O_2 diffusivity in silicone, using scaling ratios based on water diffusivities.

**Default values unless otherwise indicated.

Bulk liquid, biofilm and membrane

For both systems (MB-PBR and control) the concentrations of all the solutes in the bulk liquid were assumed constant over time. This was modeled by a fixed-concentration boundary (**Figure 2**). Initial concentrations (t=0) in the biofilm for all soluble species were assumed the same in the bulk liquid. The mass transfer resistance in the diffusion boundary layer of the biofilm was neglected.

Each solute *i* (e.g., CO_2, HCO_3^-, NO_3^-) diffuses and reacts (as appropriate) in the 1-D biofilm. The concentration of each solute over time is calculated from the **Eq. 2**, which includes the effect of diffusion and reaction, where C_i is concentration of solute *i*, D_i is diffusion coefficient and $r_{i,B}$ the net reaction rate. The net rate $r_{i,B}$ is determined by the sum of all the reaction rates derived from microbial processes and acid-base reactions (**Tables 2 and S2**) multiplied by their respective stoichiometric coefficients (**Tables 1 and S3).**

$$\frac{\partial C_i}{\partial t} = D_i \left(\frac{\partial^2 C_i}{\partial x^2} \right) + r_{i,B} \qquad (2)$$

The biofilm advective velocity, u_F (m/s), is driven by growth of phototrophic biomass and represents the physical expansion of the biofilm matrix. Assuming a constant biomass density C_x (kg COD/m^3), the biofilm advective velocity is calculated as the integration of all the microbial rates from x=0 to x=L_F, where L_F is the final biofilm thickness (m) [41]. The total growth rate for phototrophs $r_{X,B}$ (mol/(m^3 s)) results from the addition of microbial rates r_1 and r_2 (**Table 2**), e.g., growth on CO_2 and on HCO_3^-, respectively. At the biofilm base, x=0, the advective velocity is zero, so $u_{F(x=0)}$=0. Since this study considers relatively short growth cycles resulting in thin biofilms and low-shear conditions, detachment was assumed to be zero. While there probably was some degree of detachment, most likely it was negligible.

$$u_F(x) = \frac{1}{C_X} \int_0^{L_F} r_{X,B}\, dx \qquad (3)$$

The variation in biofilm thickness (L_F) over time is determined by solving the differential equation **(Eq. 4**). This equation determines the biomass velocity (u_F) at the boundary (x=L_F), resulting from biomass growth:

$$\frac{dL_F}{dt} = uF_{(x=L_F)} \qquad (4)$$

For the MB-PBR model, the gases (CO_2 and O_2) diffuse through the membrane into the biofilm, allowing it to grow on the membrane surface, while in the conventional system, the attachment surface is impermeability to gases. In the MB-PBR, the concentration gradient across the membrane wall serves as the driving force for gas transfer. The fluxes through the MB-PBR membrane are determined by Fick's law; they were implemented by transport of diluted species equations in COMSOL. In the MB-PBR model, the mass transfer coefficients were determined by the membrane's thickness and specific diffusion coefficients. Specifically, the k_m values for each gas species were calculated as the ratio of the diffusivity to the membrane thickness (D_{m_Y}/d_m), where "Y" represents the gas species (CO_2 or O_2). In the control system, there is no membrane permeability to allow the transfer of gases. Boundary conditions included a resistive flux at the membrane interface (x=0) to account for gas permeability and fixed bulk concentrations at the liquid interface (x=L_F).

2.4 Model solution

The two models (MB-PBR and control) were implemented in the COMSOL Multiphysics platform (V5.1, Comsol Inc., Burlington, MA). A system of time-dependent equations, with mass balances for solutes (**Eq. 2**), advective velocity of particulates (**Eq. 3**) which defines the internal advective velocity of the solid biomass matrix, and biofilm thickness (**Eq. 4**) which is

the rate of change of the total biofilm thickness as the biomass increases, was implemented along with corresponding boundary and initial conditions. For the MB-PBR, a mass balance for gases was included. A discretized mesh with 100 elements was used for both models. The output of the simulations included the biofilm thickness over time and profiles of concentration solutes "*S*", light intensity *I*, pH and total growth rates across the biofilm.

3. RESULTS AND DISCUSSION

3.1 Experimental results

In order to experimentally determine the MB-PBR behavior and determine key parameters, an MB-PBR and a control without CO_2 supply were operated. Once grown, three sequential, seven-day cycles of growth and biofilm harvesting were carried out. The pH was maintained by using a strong phosphate buffer in the media.

The MB-PBR biofilm grew significantly faster than the control, with increased biofilm thickness and productivity for three seven-day cycles (**Figure 3**). For the MB-PBR, the average biofilm thickness in the MB-PBR after seven days was 186±10 μm, compared to 101±10 μm for the control. The biomass productivity in the MB-PBR was 1.91±0.27 g/(m^2 d), compared to 0.49±0.06 g/(m^2 d) for the control. The increase of biomass is nearly 4-fold, while the increase in biofilm thickness is approximately 2. This discrepancy can be explained by the cylindrical geometry of the membranes. As the biofilm expands radially outward and the surface area increases, the biomass volume required to increase the thickness increases quadratically. Notably, the productivity obtained in our experiments for the MB-PBR aligns with the range of values reported in literature for phototrophic biofilms, ranging from 1 to 5 g/(m^2d) [42].

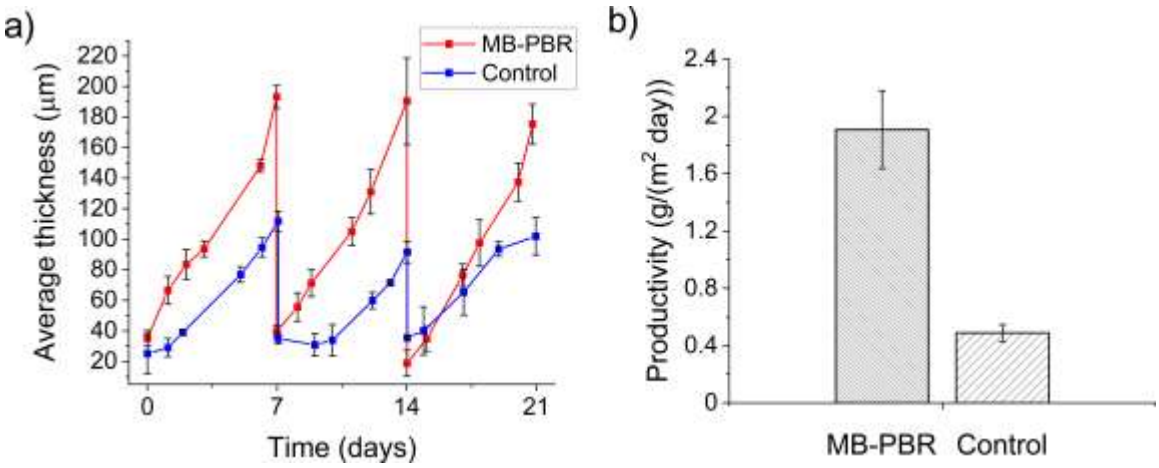

Figure 3. Biofilm behavior in three cycles of growth and harvesting for the MB-PBR and control. (a) Biofilm thickness vs. time, b) average biofilm productivities for the three cycles. Note that the initial biofilm thicknesses are approximately the same in both cases. Error bars represent the standard deviation of the three replicates.

Studies often report algal biofilm productivity in units of biomass per unit support area per unit time, e.g., g/(m^2 d). Higher productivities can be achieved in biofilm systems by minimizing inorganic carbon limitation within the biofilms, and also by preventing excessive increases in pH [43]. The MB-PBR increases growth rates by delivering inorganic carbon directly to the biofilm interior, as shown by the modeling studies. The membranes could also serve to strip dissolved oxygen from the biofilm, enhancing the growth rates by avoiding oxygen accumulation. Previous studies have used membranes for carbonation of the media, as support carrier, and to separate algae from the liquid [44,45]. However, the CO_2 delivery is still from the bulk liquid to the biofilm.

Prior research has shown that a buffer can increase algal uptake of dissolved inorganic carbon [46,47], which supports our experimental results. Inorganic carbon speciation profiles across the biofilm are dynamic and pH-dependent [48]. Thus, maintaining a stable pH is important for

inorganic carbon delivery. Large increases in pH can potentially decrease the growth rates, since it reduces inorganic carbon availability. It also can affect the growth rate if outside the optimal pH range.

3.2 Parameter estimation

Reported values for the light attenuation coefficient (k_e) and the half-saturation coefficient of light irradiance (K_I) have a high degree of variability. Reported k_e values range from 1,000 to 83,334 1/m [49–54] and reported K_I range from 4.2 to 83.22 W/m² [55–59]. Since our sensitivity analysis showed our model to be sensitive to both parameters (see **Table S4**), we used our first two experimental data sets to determine the best-fit values. These were k_e=80,000 1/m and K_I=5 W/m^2 (**Figure S3**, **Table S5**), which fall within the range of reported values. After validating our model with the third data set (**Figure S4**), the calibrated model was used in our simulations. The average relative error (%) for MB-PBR was calculated as 11.45% and for the control as 17.70%.

3.3 Effect of CO_2 supply concentration

Carbon is a key nutrient for production of algal biomass [4], and it may be more limiting for biofilm reactors than suspended growth. Reported microalgal productivities range from 4 - 20 g/(m^2 d) for open ponds (suspended growth), but only 1 - 5 g/(m^2 d) for algal biofilm reactors [42]. The lower productivity likely due to CO_2 limitation within the biofilm, although it also may be due to pH shifts within the biofilm.

Biofilm growth for the MB-PBR and the control reactor were simulated with the 1-D model (**Fig. 4a**). In the MB-PBR model, the gas supply was 5% CO_2 and 95% N_2 and the light

intensity was 18.5 W/m^2, as with the experimental reactor. The bulk water, e.g., the fixed concentration boundary on the outer biofilm, was assumed to be in equilibrium with atmospheric CO_2. The initial biofilm thickness was 30 µm.

After seven days of growth, the predicted MB-PBR biofilm thickness was 176 µm, while the control was only 90 µm (**Fig. 4a**). The terms for oxygen and light inhibition on growth rates were inactivated for these simulations to study the effect of CO_2 supply alone. The profiles of O_2, CO_2, light intensity, pH and growth rates for both systems, at biofilm thicknesses of 80 µm, are shown in **Fig. 4b and 4c.** The growth rate presented in **Fig. 4** is the total combined rate on CO_2 (r_1) and on HCO_3^- (r_2). The profiles across the biofilm (x) were simulated with thicknesses of 80-100 µm to prevent light limitation in the biofilm interior.

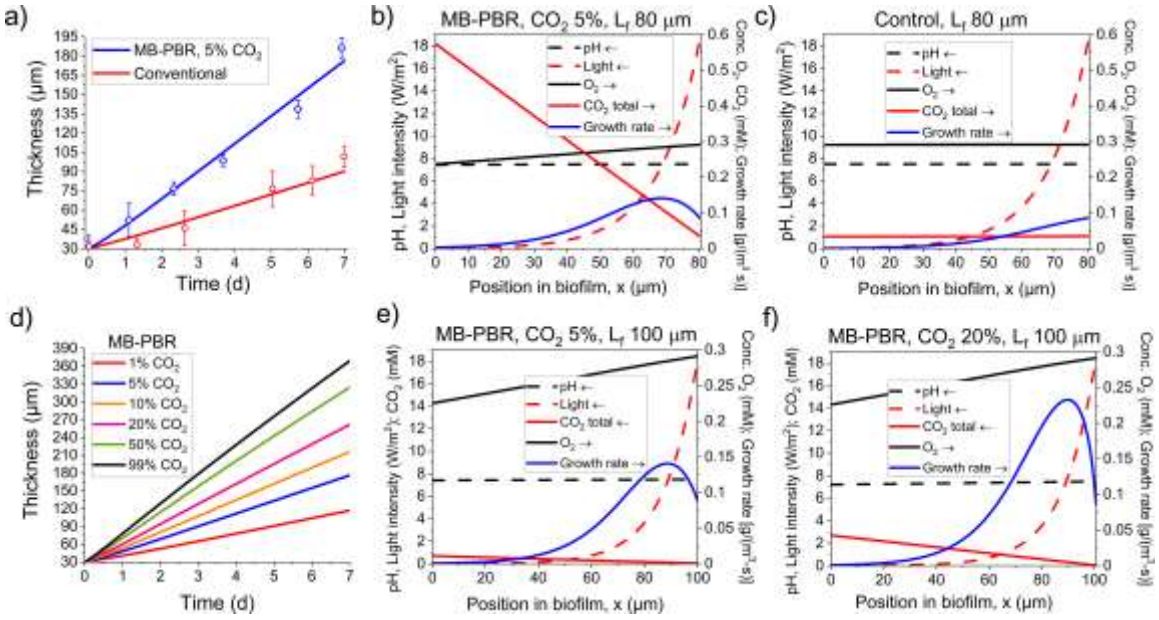

Figure 4. Comparison of MB-PBR and conventional biofilm system performance, and effects of CO_2 supply pressure on MB-PBR performance. Panels a, b and c compare the MB-PBR with the control system, where the MB-PBR is supplied with 5% CO_2. Panel a) shows the biofilm thicknesses of both systems compared to the average experimental values (dots), while panels b) and c) show the profiles of pH, light, oxygen, CO_2 concentrations and growth rates. Panels d, e and f compare different CO_2 supply concentrations in the MB-PBR system. Similar to the above panels, panel d) shows biofilm thicknesses for different CO_2 concentrations supplied in the MB-PBR, while panels e) and f) shows the profiles of two selected CO_2

418 percentages (5% and 20%). Panels b) to f) are exclusively modeling outputs. Simulation times
419 were chosen to provide a thickness of 80-100 μm in all cases. To allow this, given the different
420 growth rates, the profiles were provided for the following times: (4b) t=2.5 d; (4c) t=5.9 d; (4e)
421 t=3.5 d; (4f) t=2.2 d.
422

423 The simulated light profiles with the biofilm were similar for both systems. Since the media
424 was well buffered (16 mM total PO_4^{3-}), the pH profiles were flat. Since oxygen and light
425 inhibition were not included, the growth rate was affected only by the light and inorganic
426 carbon limitation.
427

428 In the control, the simulated growth rates were significantly lower than for the MB-PBR. The
429 maximum growth rate, 0.086 g/(m^3 s), was in the outer biofilm, where the inorganic carbon is
430 present as bulk-liquid bicarbonate. For the MB-PBR, the maximum growth rate was higher,
431 0.141 g/(m^3 s), and was located in the biofilm interior, closer to the CO_2 supply from the
432 membrane (**Figures 4b and 4c**).
433

434 The availability of inorganic carbon in the control can only be increased by increasing the bulk
435 inorganic carbon concentration, e.g., by adding bicarbonate to the bulk liquid. However, the
436 inorganic carbon concentration in the MB-PBR can also be increased by increasing the CO_2
437 partial pressure across the membrane, or increasing the percentage of CO_2 in the membrane gas.
438 Recarbonation from atmospheric CO_2 is typically insufficient to match demands from rapid
439 culture [60]. And adding bicarbonate in the media, in some cases, is ineffective in increasing algal
440 biomass growth and nutrient removal in algal biofilms [61]. Regardless, adding bicarbonate can
441 be a significant cost, and some will be lost with the reactor effluent, resulting in poor utilization
442 efficiency.

443

444 Dissolved inorganic carbon can exist as H_2CO_3 (dissolved CO_2), HCO_3^- and CO_3^{2-}. CO_2 is the
445 preferred substrate for photosynthesis, but HCO_3^- also can be used and converted to CO_2 before
446 uptake or intracellularly [48]. To understand the effect of CO_2 concentration on MB-PBR
447 performance, a parametric sweep on the CO_2 fraction in the supply gas was carried out. The
448 simulated CO_2 volumetric fractions, y_{CO2}, were 1%, 5%, 10%, 20%, 50% and 99% (**Figure 4d**).
449 After seven days of growth, higher biofilm thicknesses were obtained for higher CO_2
450 concentrations in the membrane. For example, without CO_2 (control) the thickness was 90 μm.
451 A thickness of 117 μm was obtained with 1% CO_2, and 176 μm with 5%. A thickness of 369
452 μm was obtained with 99% CO_2. Note that there were diminishing returns for y_{CO2} fractions
453 above 5%. This was because increasing the CO_2 from 1 to 5% allows more CO_2 to reach the
454 biofilm's photic zone (outer biofilm). But further increases in the CO_2 supply concentration
455 only makes a small difference to areas already receiving CO_2, and only slightly expand CO_2
456 penetration into the outer, CO_2-limited region of the photic zone. **Fig. 4e** and **4f** compare the
457 profiles for 5% and 20% CO_2. The plot for 20% CO_2 shows significantly higher growth rates
458 within the biofilm than that for 5% CO_2.
459

460 For suspended culture and biofilms, the CO_2 fractions for optimal algal growth are reported to
461 be 1 to 5% [62,63]. It is generally accepted that microalgae are sensitive to very high CO_2 levels.
462 However, it has been shown that some microalgae can grow rapidly under CO_2 concentrations
463 up to 40% and some species can grow even at 100% CO_2 (e.g. *Chlorella* sp. T-1) [64,65].
464 Acclimation to low or high CO_2 concentrations might play an important role in the
465 photosynthetic rates at different CO_2 concentrations. Unicellular green algae and cyanobacteria

466 are naturally adapted to the low CO_2 atmospheric levels (0.038%), using an inorganic carbon
467 concentration mechanism (CCM). This mechanism is suppressed at elevated levels of CO_2 of 1-
468 5%, [66]. When microalgal cells are grown under high CO_2 concentrations, e.g., 5%, even when
469 there is a suppression of the CCM, the maximum photosynthesis rate is increased in some
470 genera, such as *Chlorella*, but not in others, such as *Chlamydomonas* [67]. Using elevated CO_2
471 levels can improve growth rates up to a point. The photosynthetic rate increase will depend on
472 the algal species, acclimation stage and other culture conditions. While using waste CO_2, e.g.,
473 from an industrial process, could provide substantial cost benefits, further study is needed to
474 understand the impact of impurities. Otherwise, the cost of using commercial grade gas is an
475 additional factor to consider [68].
476 A practical application of this model is, for a given incident light intensity, water buffering, and
477 CO_2 in the liquid and membrane supply, determining the ideal strategies for biofilm harvesting.
478 Harvesting too much biofilm can result in low initial growth rate of new biofilm. On the other
479 hand, allowing the biofilm to become too thick reduces the benefit CO_2 supply from the
480 membrane, as the CO_2 concentration at the outer biofilm may be too low.
481
482 3.4 Effect of pH
483 Biofilms provide micro-environments where their pH values can differ from the bulk
484 environment [69]. To study the effect of pH and phosphate buffer strength on MB-PBR, oxygen
485 and light inhibition were again neglected. The CO_2 gas concentration in the membrane was 5%
486 and the phosphate buffer addition was simulated as 16 mM or 0.023 mM (phosphate present in
487 the BG-11 media, no extra buffer added). The light intensity was increased to 250 W/m^2 and
488 initial pH was 7.5. Using phosphate buffer enhanced the biofilm growth after 21 days, but a

counter-effect was observed during the first stages of growth, where the "No buffer" condition presented a slightly higher thickness (**Fig. 5a**). This could be explained by observing the profiles for pH, CO_2 total and carbon species (**Fig. 5b and 5c).**

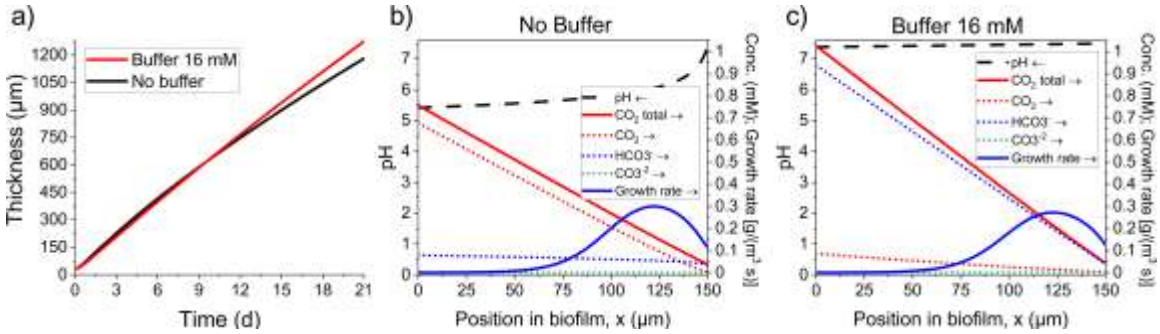

Figure 5. Effect of pH on MB-PBR, via modeling. Panels (a, b, c) compare a phosphate-buffered MB-PBR with a MB-PBR without phosphate buffer. Panel a) shows the biofilm thicknesses, while panels b) and c) show the pH, CO_2 total, carbon species and growth rates for both biofilms simulated on both conditions. Simulation times to provide a 150 µm thickness: (5a) t=21 d; (5b) t=1.9 d; (5c) t=2.1 d.

When the phosphate buffer is lacking, the pH decreases to 5.4 at the base of the biofilm, affecting the total CO_2. Without buffer and with a pH of 5.4, the CO_2 remains mostly in its dissolved form (CO_2(aq)) rather than converting to bicarbonate (HCO_3^-) or carbonate (CO_3^{2-}). In the buffered system with a pH of 7.38 at the base of the biofilm, a significant portion of CO_2 is converted to bicarbonate. Bicarbonate can be utilized by microalgae, but it also represents a more stable storage form of inorganic carbon. The lower pH in the non-buffered condition may increase the concentration of dissolved CO_2.

In addition to affecting inorganic carbon speciation, the pH can adversely affect the growth rates for $5.5 \leq pH \leq 8.5$. In the non-buffered condition, the higher availability of CO_2(aq) compensates for potential low pH inhibition, resulting in a net increase in growth rates in the first stages of growth. Microalgal growth is optimal at pH values between 6 and 9. Low pH

might induce cytoplasm and chloroplast acidification, decreasing photosynthetic rates [67]. The pH is also important for biofilm establishment (not included in this model), since it influences the production of extracellular polymeric substances (EPS), such as proteins, polysaccharides and lipids [13]. Furthermore, adhesion can be enhanced at pH≥7 in diatoms, chlorophytes and cyanobacteria [70].

The above suggest that, while a moderate acidification (e.g., pH 5.4) observed in the non-buffered condition can initially favor growth by increasing the dissolved CO_2, it presents a narrow operational window. In the absence of a buffering system, any further increase in CO_2 supply poses a risk of dropping the pH below physiological limits (pH 3 - 4), potentially decreasing growth rates.

3.5 Photoinhibition

Light is the driving force for photosynthesis, and it also plays important role in the assimilation of nutrients and the EPS composition phototrophic biofilms [71]. If little light is available in the deeper biofilm, this zone will experience photo limitation. However, if the light intensity is excessively high, typically in the outer biofilm, photoinhibition occurs. The extent of photolimitation or photoinhibition depend greatly on the biofilm composition and growth conditions. Light can inhibit growth at irradiances above 30 W/m^2 [72]. Other authors have reported light saturation (no longer be rate limiting) at 60, 100 and 150 $\mu mol/(m^2\ s)$ (13, 22 and 33 W/m^2, respectively) and others considered light limitation between 12 - 88 $\mu mol/(m^2\ s)$ (2.6 – 19 W/m^2) [73].

In this study, light inhibition was modeled with a self-inhibition term (I^2/K_{LI}). Rates are presented in **Table 2**. Simulations for a MB-PBR system were performed with and without a light inhibition term (**Fig. 6a**). A high light intensity was used (200 W/m^2), the CO_2 supplied in the membrane was at 5%, and the light inhibition coefficient was K_{LI}=50 W/m^2. As expected, light inhibition decreased biofilm growth rates. A high light intensity has the potential to negatively impact the activity rates on the outer surface of the biofilm as it is shown by the profiles comparing both conditions (**Fig. 6b and 6c**).

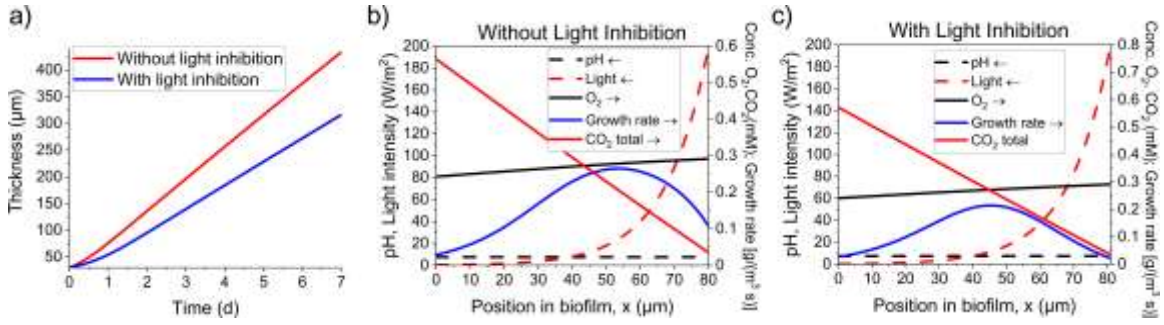

Figure 6. Assessment of light inhibition in the MB-PBR, via modeling. MB-PBR without and with light inhibition term added were compared in terms of biofilm thickness (6a) and profiles across the biofilm (6b and 6c). Simulation times for reaching 80 μm thickness: (6b) t=1.1 d; (6c) t=1.7 d.

In suspended cultures, most of the light absorption is from algal cells close to the water surface, creating a self-shading effect and a light gradient in photobioreactors. This phenomenon can also occur in biofilms, where cells are more densely packed [74]. Similar to suspended cultures, algal biofilms cells absorb almost all of the photons they receive. However, they cannot use all the energy, instead, the excess is dissipated through mechanisms such as non-photochemical quenching, reactive oxygen species (ROS) generation and fluorescence [75,76], blocking the inner cells from receiving enough light for growth. As the biofilm grows thick, the deeper cells cannot obtain enough light for photosynthesis [4], creating a photosynthetically inactive region.

This effect has been largely demonstrated by measuring the photo flux density (PFD) of a biofilm: cells adjacent to the light source were receiving high PFD, but cells in the inner biofilm at a distance of 150 μm were almost in dark conditions [77]. Other studies report that light can penetrate around 200 μm into biofilms [78], which is in general accordance with our model: for both conditions, light is still present around 0.3 W/m^2 in the deeper regions of the biofilms.

A potential limitation of the MB-PBR is the counter-directional supply of light, nutrients, and CO_2. In extremely thick biofilms, this could lead to stratified inactive zones where light, carbon or nutrients might be limiting. Despite this, the MB-PBR offers some advantages that compensate for this constraint, such as near 100% gas transfer efficiency (minimizing losses associated with sparging CO_2 to the bulk); oxygen removal from the biofilm via back-diffusion and capability of a dual supply of CO_2 if coupled with bicarbonate in the bulk. In addition, this limitation can be easily managed through operational control by implementing periodic harvesting of the biomass, maintaining an active biofilm.

In this research, our experiments were based on a synthetic minimal medium, and our model only included phototrophic organisms. In reality, algal photobioreactors could be supplied with water containing organic carbon, particulate matter, color and turbidity. More complex, multispecies models (e.g., including heterotrophic bacteria) might be needed to address more realistic conditions.

CONCLUSIONS

We developed a new algal biofilm model that capture the behavior of phototrophic biofilms growing on a counter-diffusional, CO_2 supplying membrane. Following calibration, the model successfully predicted the growth rates of our experimental system, and allowed us to obtain new insights into its behavior. Our results show that the MB-PBR can significantly enhance phototrophic biomass production rates. Experiments showed a 3.9-fold increase in biomass productivity with CO_2 supply. Our simulations suggest that buffer addition in the bulk liquid can help prevent dramatic pH shifts in the biofilm interior, and that light becomes limiting (inner biofilm) or inhibitory (outer biofilm) at certain threshold of biofilm thicknesses, depending on the light intensity. This work provides a more fundamental understanding of membrane algal biofilms and highlights the MB-PBR's potential for diverse applications, such as wastewater treatment, biofuel production and CO_2 capture. It also provides a tool to determine optimal biomass harvesting strategies. Future work should explore the effect of the MB-PBR on the biofilm microbial ecology, harvesting strategies, photobioreactor geometry and arrangement of membranes, predation within the biofilm, light supply, among others.

Acknowledgements

We appreciate financial support from the Notre Dame seed grant program. We also acknowledge initial guidance with the biofilm model from Cristian Picioreanu at KAUST.

Supporting Information

Additional modeling and experimental details, materials, and methods, including photographs of experimental setup (DOC).

REFERENCES

(1) Mata, T. M.; Caetano, Nidia. S.; Martins, A. A. Microalgae for Biodiesel Production and Other Applications: A Review. *Renewable and Sustainable Energy Reviews*. 2010, pp 217–232. https://doi.org/10.1016/j.rser.2009.07.020

(2) Brune, D. E.; Lundquist, T. J.; Benemann, J. R. Microalgal Biomass for Greenhouse Gas Reductions: Potential for Replacement of Fossil Fuels and Animal Feeds. *Journal of Environmental Engineering* 2009, *135* (11), 1136–1144. https://doi.org/10.1061/(ASCE)EE.1943-7870.0000100

(3) Strieth, D.; Ulber, R.; Muffler, K. Application of Phototrophic Biofilms: From Fundamentals to Processes. *Bioprocess and Biosystems Engineering*. Springer Verlag March 1, 2018, pp 295–312. https://doi.org/10.1007/s00449-017-1870-3

(4) Hoh, D.; Watson, S.; Kan, E. Algal Biofilm Reactors for Integrated Wastewater Treatment and Biofuel Production: A Review. *Chemical Engineering Journal* 2016, *287*, 466–473. https://doi.org/10.1016/j.cej.2015.11.062

(5) Gross, M.; Jarboe, D.; Wen, Z. Biofilm-Based Algal Cultivation Systems. *Appl. Microbiol. Biotechnol.* 2015, *99* (14), 5781–5789. https://doi.org/10.1007/s00253-015-6736-5

(6) Ozkan, A.; Kinney, K.; Katz, L.; Berberoglu, H. Reduction of Water and Energy Requirement of Algae Cultivation Using an Algae Biofilm Photobioreactor. *Bioresour. Technol.* 2012, *114*, 542–548. https://doi.org/10.1016/j.biortech.2012.03.055

(7) Wang, J.; Liu, W.; Liu, T. Biofilm Based Attached Cultivation Technology for Microalgal Biorefineries—A Review. *Bioresour. Technol.* 2017, *244*, 1245–1253. https://doi.org/10.1016/j.biortech.2017.05.136

(8) Zhuang, L. L.; Yu, D.; Zhang, J.; Liu, F. fei; Wu, Y. H.; Zhang, T. Y.; Dao, G. H.; Hu, H. Y. The Characteristics and Influencing Factors of the Attached Microalgae Cultivation: A Review. *Renewable and Sustainable Energy Reviews* 2018, *94* (November 2017), 1110–1119. https://doi.org/10.1016/j.rser.2018.06.006

(9) Kumar, A.; Yuan, X.; Sahu, A. K.; Dewulf, J.; Ergas, S. J.; Langenhove, H. van. A Hollow Fiber Membrane Photo-Bioreactor for CO2 Sequestration from Combustion Gas Coupled with Wastewater Treatment: A Process Engineering Approach. *Journal of Chemical Technology & Biotechnology* 2010, *85* (3), 387–394. https://doi.org/10.1002/JCTB.2332

(10) Ferreira, B.; Fernandes, H.; Reis, A.; Mateus, M. Microporous Hollow Fibres for Carbon Dioxide Absorption: Mass Transfer Model Fitting and the Supplying of Carbon Dioxide to Microalgal Cultures. *Journal of Chemical Technology & Biotechnology* 1998. https://doi.org/10.1002/(SICI)1097-4660(199801)71:1

(11) Kim, H. W.; Cheng, J.; Rittmann, B. E. Direct Membrane-Carbonation Photobioreactor Producing Photoautotrophic Biomass via Carbon Dioxide Transfer and Nutrient Removal. *Bioresour. Technol.* 2016, *204*, 32–37. https://doi.org/10.1016/J.BIORTECH.2015.12.066

(12) Hajinajaf, N.; Fallahi, A.; Eustance, E.; Sarnaik, A.; Askari, A.; Najafi, M.; Davis, R. W.; Rittmann, B. E.; Varman, A. M. Managing Carbon Dioxide Mass Transfer in Photobioreactors for Enhancing Microalgal Biomass Productivity. *Algal Res.* 2024, *80*, 103506. https://doi.org/10.1016/J.ALGAL.2024.103506

(13) Mantzorou, A.; Ververidis, F. Microalgal Biofilms: A Further Step over Current Microalgal Cultivation Techniques. *Science of the Total Environment*. Elsevier B.V. February 15, 2019, pp 3187–3201. https://doi.org/10.1016/j.scitotenv.2018.09.355

(14) Mathew, M. M.; Khatana, K.; Vats, V.; Dhanker, R.; Kumar, R.; Dahms, H. U.; Hwang, J. S. Biological Approaches Integrating Algae and Bacteria for the Degradation of Wastewater

Contaminants—A Review. *Frontiers in Microbiology*. Frontiers Media S.A. February 3, 2022. https://doi.org/10.3389/fmicb.2021.801051

(15) Baba, M.; Shiraiwa, Y. High-CO 2 Response Mechanisms in Microalgae. 2007, *2*.

(16) Zheng, Q.; Xu, X.; Martin, G. J. O.; Kentish, S. E. Critical Review of Strategies for CO2 Delivery to Large-Scale Microalgae Cultures. *Chinese Journal of Chemical Engineering*. Chemical Industry Press November 1, 2018, pp 2219–2228. https://doi.org/10.1016/j.cjche.2018.07.013

(17) David, C.; Bühler, K.; Schmid, A. Stabilization of Single Species Synechocystis Biofilms by Cultivation under Segmented Flow. *J. Ind. Microbiol. Biotechnol.* 2015, *42* (7), 1083–1089. https://doi.org/10.1007/S10295-015-1626-5

(18) Li, T.; Podola, B.; Melkonian, M. Investigating Dynamic Processes in a Porous Substrate Biofilm Photobioreactor — A Modeling Approach. *Algal Res.* 2016, *13*, 30–40. https://doi.org/10.1016/J.ALGAL.2015.11.006

(19) Li, T.; Piltz, B.; Podola, B.; Dron, A.; de Beer, D.; Melkonian, M. Microscale Profiling of Photosynthesis-Related Variables in a Highly Productive Biofilm Photobioreactor. *Biotechnol. Bioeng.* 2016, *113* (5), 1046–1055. https://doi.org/10.1002/BIT.25867

(20) Guo, C.; Duan, D.; Sun, Y.; Han, Y.; Zhao, S. Enhancing Scenedesmus Obliquus Biofilm Growth and CO2 Fixation in a Gas-Permeable Membrane Photobioreactor Integrated with Additional Rough Surface. *Algal Res.* 2019, *43*. https://doi.org/10.1016/j.algal.2019.101620

(21) Ding, K.; Wang, N.; Huang, X.; Liao, C.; Liu, S.; Yang, M.; Wang, Y. Z. Enhancing Lipid Productivity with Novel SiO2-Modified Polytetrafluoroethylene (PTFE) Membranes in a Membrane Photobioreactor. *Algal Res.* 2020, *45*. https://doi.org/10.1016/j.algal.2019.101752

(22) Semmens, M. J.; Essila, N. J.; Member, A. *MODELING BIOFILMS ON GAS-PERMEABLE SUPPORTS: FLUX LIMITATIONS*; 2001.

(23) Pérez-Calleja, P.; Clements, E.; Nerenberg, R. Enhancing Ammonium Oxidation Fluxes and Nitritation Efficiencies in MABRs: A Modeling Study. *Environ. Sci. (Camb).* 2022, *8* (2), 358–374. https://doi.org/10.1039/D1EW00337B

(24) Wang, R.; Terada, A.; Lackner, S.; Smets, B. F.; Henze, M.; Xia, S.; Zhao, J. Nitritation Performance and Biofilm Development of Co- and Counter-Diffusion Biofilm Reactors: Modeling and Experimental Comparison. *Water Res.* 2009, *43* (10), 2699–2709. https://doi.org/10.1016/J.WATRES.2009.03.017

(25) Martin, K. J.; Picioreanu, C.; Nerenberg, R. Multidimensional Modeling of Biofilm Development and Fluid Dynamics in a Hydrogen-Based, Membrane Biofilm Reactor (MBfR). *Water Res.* 2013, *47* (13), 4739–4751. https://doi.org/10.1016/J.WATRES.2013.04.031

(26) Aparicio, S.; González-Camejo, J.; Seco, A.; Borrás, L.; Robles, Á.; Ferrer, J. Integrated Microalgae-Bacteria Modelling: Application to an Outdoor Membrane Photobioreactor (MPBR). *Science of The Total Environment* 2023, *884*, 163669. https://doi.org/https://doi.org/10.1016/j.scitotenv.2023.163669

(27) Wolf, G.; Picioreanu, C.; Loosdrecht, M. C. M. Van. Kinetic Modeling of Phototrophic Biofilms : The PHOBIA Model. 2007, *97* (5), 1064–1079. https://doi.org/10.1002/bit

(28) Liu, M.; Liao, B. Modelling of Diffusion and Reaction of Carbon Dioxide and Nutrients in Biofilm for Optimal Design and Operation of Emerging Membrane Carbonated Microalgal Biofilm Photobioreactors. *Membranes (Basel).* 2025, *15* (9). https://doi.org/10.3390/membranes15090269

(29) Rippka, E.; Deruelles, J.; Waterbury, N. B. *Generic Assignments, Strain Histories and Properties of Pure Cultures of Cyanobacteria*; 1979; Vol. 111.

(30) Perez-Calleja, P.; Aybar, M.; Picioreanu, C.; Esteban-Garcia, A. L.; Martin, K. J.; Nerenberg, R. Periodic Venting of MABR Lumen Allows High Removal Rates and High Gas-Transfer Efficiencies. *Water Res.* 2017, *121*, 349–360. https://doi.org/10.1016/j.watres.2017.05.042

(31) Lewandowski, Z.; Beyenal, H. *Fundamentals of Biofilm Research*, 2nd ed.; CRC press, 2007.

(32) Shoener, B. D.; Schramm, S. M.; Béline, F.; Bernard, O.; Martínez, C.; Plósz, B. G.; Snowling, S.; Steyer, J. P.; Valverde-Pérez, B.; Wágner, D.; Guest, J. S. Microalgae and Cyanobacteria Modeling in Water Resource Recovery Facilities: A Critical Review. *Water Res. X* 2019, *2*, 100024. https://doi.org/10.1016/J.WROA.2018.100024

(33) Čatský, J. Langhans, R.W., Tibbitts, T.W. (Ed.): Plant Growth Chamber Handbook. *Photosynthetica* 1998, *35* (2), 232. https://doi.org/10.1023/A:1006995714717

(34) Ebrahimi, S.; Picioreanu, C.; Kleerebezem, R.; Heijnen, J. J.; van Loosdrecht, M. C. M. Rate-Based Modelling of SO2 Absorption into Aqueous NaHCO3/Na2CO3 Solutions Accompanied by the Desorption of CO2. *Chem. Eng. Sci.* 2003, *58* (16), 3589–3600. https://doi.org/10.1016/S0009-2509(03)00231-8

(35) Picioreanu, C.; Van Loosdrecht, M. C. M.; Heijnen, J. J. Modelling the Effect of Oxygen Concentration on Nitrite Accumulation in a Biofilm Airlift Suspension Reactor. *Water Science and Technology* 1997, *36* (1), 147–156. https://doi.org/10.1016/S0273-1223(97)00347-8

(36) Cussler, E. Diffusion: Mass Transfer in Fluid Systems. 2009.

(37) Vanysek, P. *CRC Handbook of Chemistry and Physics*, 86nd ed.; LLC, C. P., Ed.; Boca Raton, 2001.

(38) Cox, M. E.; Dunn, B. *Oxygen Diffusion in Poly(Dimethy1 Siloxane) Using Fluorescence Quenching. I. Measurement Technique and Analysis*.

(39) Ding, C.; Fan, Y. Measurement of Diffusion Coefficients of Air in Silicone Oil and in Hydraulic Oil. *Chin. J. Chem. Eng.* 2011, *19* (2), 205–211. https://doi.org/10.1016/S1004-9541(11)60155-9

(40) Atkins, P.; De Paula, J. *Elements of Physical Chemistry*, 4th ed.; W.H. Freeman, 2005.

(41) Eberl, H.; Morgenroth, E.; Noguera, D.; Picioreanu, C.; Rittman, B.; Van Loosdrecht, M.; Wanner, O. *Mathematical Modeling of Biofilms*; IWA Publishing, 2006. https://doi.org/10.2166/9781780402482

(42) Roostaei, J.; Zhang, Y.; Gopalakrishnan, K.; Ochocki, A. J. Mixotrophic Microalgae Biofilm: A Novel Algae Cultivation Strategy for Improved Productivity and Cost-Efficiency of Biofuel Feedstock Production. *Sci. Rep.* 2018, *8* (1), 1–10. https://doi.org/10.1038/s41598-018-31016-1

(43) Gross, M.; Wen, Z. Yearlong Evaluation of Performance and Durability of a Pilot-Scale Revolving Algal Biofilm (RAB) Cultivation System. *Bioresour. Technol.* 2014, *171*, 50–58. https://doi.org/10.1016/j.biortech.2014.08.052

(44) Gao, F.; Yang, Z. H.; Li, C.; Zeng, G. M.; Ma, D. H.; Zhou, L. A Novel Algal Biofilm Membrane Photobioreactor for Attached Microalgae Growth and Nutrients Removal from Secondary Effluent. *Bioresour. Technol.* 2015, *179*, 8–12. https://doi.org/10.1016/j.biortech.2014.11.108

(45) Rahaman, M. S. A.; Cheng, L.-H.; Xu, X.-H.; Zhang, L.; Chen, H.-L. A Review of Carbon Dioxide Capture and Utilization by Membrane Integrated Microalgal Cultivation Processes. *Renewable and Sustainable Energy Reviews* 2011, *15* (8), 4002–4012. https://doi.org/10.1016/j.rser.2011.07.031

(46) Keymer, P. C.; Lant, P. A.; Pratt, S. Modelling Microalgal Activity as a Function of Inorganic Carbon Concentration: Accounting for the Impact of PH on the Bicarbonate System. *J. Appl. Phycol.* 2014, *26* (3), 1343–1350. https://doi.org/10.1007/s10811-013-0146-9

(47) Nguyen, B. T.; Rittmann, B. E. Predicting Dissolved Inorganic Carbon in Photoautotrophic Microalgae Culture via the Nitrogen Source. *Environ. Sci. Technol.* 2015, *49* (16), 9826–9831. https://doi.org/10.1021/acs.est.5b01727

(48) Li, T.; Strous, M.; Melkonian, M. Biofilm-Based Photobioreactors: Their Design and Improving Productivity through Efficient Supply of Dissolved Inorganic Carbon. *FEMS Microbiology Letters*. Oxford University Press December 1, 2017. https://doi.org/10.1093/femsle/fnx218

(49) Li, T.; Piltz, B.; Podola, B.; Dron, A.; de Beer, D.; Melkonian, M. Microscale Profiling of Photosynthesis-Related Variables in a Highly Productive Biofilm Photobioreactor. *Biotechnol. Bioeng.* 2016, *113* (5), 1046–1055. https://doi.org/10.1002/BIT.25867

(50) Huang, J.; Chu, R.; Chang, T.; Cheng, P.; Jiang, J.; Yao, T.; Zhou, C.; Liu, T.; Ruan, R. Modeling and Improving Arrayed Microalgal Biofilm Attached Culture System. *Bioresour. Technol.* 2021, *331*, 124931. https://doi.org/10.1016/J.BIORTECH.2021.124931

(51) Bara, O.; Bonnefond, H.; Bernard, O. Model Development and Light Effect on a Rotating Algal Biofilm. *IFAC-PapersOnLine* 2019, *52* (1), 376–381. https://doi.org/10.1016/J.IFACOL.2019.06.091

(52) Flora, J. R. V.; Suidan, M. T.; Biswas, P.; Sayles, G. D. Modeling Algal Biofilms: Role of Carbon, Light, Cell Surface Charge, and Ionic Species. *Water Environment Research* 1995, *67* (1), 87–94. https://doi.org/10.2175/106143095X131222

(53) Ma, S.; Huang, Y.; Zhang, B.; Zhu, X.; Xia, A.; Zhu, X.; Liao, Q. Comprehensive Modeling and Predicting Light Transmission in Microalgal Biofilm. *J. Environ. Manage.* 2023, *326*, 116757. https://doi.org/10.1016/J.JENVMAN.2022.116757

(54) Straka, L.; Rittmann, B. E. Light Attenuation Changes with Photo-Acclimation in a Culture of Synechocystis Sp. PCC 6803. *Algal Res.* 2017, *21*, 223–226. https://doi.org/10.1016/J.ALGAL.2016.11.024

(55) Feng, F.; Li, Y.; Latimer, B.; Zhang, C.; Nair, S. S.; Hu, Z. Prediction of Maximum Algal Productivity in Membrane Bioreactors with a Light-Dependent Growth Model. *Science of The Total Environment* 2021, *753*, 141922. https://doi.org/10.1016/J.SCITOTENV.2020.141922.

(56) Straka, L.; Rittmann, B. E. Light Attenuation Changes with Photo-Acclimation in a Culture of Synechocystis Sp. PCC 6803. *Algal Res.* 2017, *21*, 223–226. https://doi.org/10.1016/J.ALGAL.2016.11.024

(57) Liehr, S. K.; Suidan, M. T.; Eheart, J. W. A Modeling Study of Carbon and Light Limitation in Algal Biofilms. *Biotechnol. Bioeng.* 1990, *35* (3), 233–243. https://doi.org/10.1002/BIT.260350304

(58) Muñoz Sierra, J. D.; Picioreanu, C.; Van Loosdrecht, M. C. M. Modeling Phototrophic Biofilms in a Plug-Flow Reactor. *Water Science and Technology* 2014, *70* (7), 1261–1270. https://doi.org/10.2166/WST.2014.368

(59) Ye, Y.; Ma, S.; Peng, H.; Huang, Y.; Zeng, W.; Xia, A.; Zhu, X.; Liao, Q. Insight into the Comprehensive Effect of Carbon Dioxide, Light Intensity and Glucose on Heterotrophic-Assisted Phototrophic Microalgae Biofilm Growth: A Multifactorial Kinetic Model. *J. Environ. Manage.* 2023, *325*, 116582. https://doi.org/10.1016/J.JENVMAN.2022.116582

(60) Sebestyén, P.; Blanken, W.; Bacsa, I.; Tóth, G.; Martin, A.; Bhaiji, T.; Dergez, Á.; Kesseru, P.; Koós, Á.; Kiss, I. Upscale of a Laboratory Rotating Disk Biofilm Reactor and Evaluation of Its Performance over a Half-Year Operation Period in Outdoor Conditions. *Algal Res.* 2016, *18*, 266–272. https://doi.org/10.1016/j.algal.2016.06.024

(61) Kesaano, M.; Gardner, R. D.; Moll, K.; Lauchnor, E.; Gerlach, R.; Peyton, B. M.; Sims, R. C. Dissolved Inorganic Carbon Enhanced Growth, Nutrient Uptake, and Lipid Accumulation in Wastewater Grown Microalgal Biofilms. *Bioresour. Technol.* 2015, *180*, 7–15. https://doi.org/10.1016/j.biortech.2014.12.082

(62) Zhang, H.; Gong, W.; Bai, L.; Chen, R.; Zeng, W.; Yan, Z.; Li, G.; Liang, H. Aeration-Induced CO2 Stripping, Instead of High Dissolved Oxygen, Have a Negative Impact on Algae–Bacteria Symbiosis (ABS) System Stability and Wastewater Treatment Efficiency. *Chemical Engineering Journal* 2020, *382*, 122957. https://doi.org/10.1016/j.cej.2019.122957

(63) Cheng, L.; Zhang, L.; Chen, H.; Gao, C. Carbon Dioxide Removal from Air by Microalgae Cultured in a Membrane-Photobioreactor. *Sep. Purif. Technol.* 2006, *50* (3), 324–329. https://doi.org/10.1016/j.seppur.2005.12.006

(64) Zhao, B.; Su, Y. Process Effect of Microalgal-Carbon Dioxide Fixation and Biomass Production: A Review. *Renewable and Sustainable Energy Reviews*. Elsevier Ltd March 1, 2014, pp 121–132. https://doi.org/10.1016/j.rser.2013.11.054

(65) Cheah, W. Y.; Show, P. L.; Chang, J. S.; Ling, T. C.; Juan, J. C. Biosequestration of Atmospheric CO2 and Flue Gas-Containing CO2 by Microalgae. *Bioresource Technology*. Elsevier Ltd May 1, 2015, pp 190–201. https://doi.org/10.1016/j.biortech.2014.11.026

(66) Ghoshal, D.; Goyal, A. Oxygen Inhibition of Dissolved Inorganic Carbon Uptake in Unicellular Green Algae. *Phycological Res.* 2001, *49* (4), 319–324. https://doi.org/10.1046/j.1440-1835.2001.00247.x

(67) Miyachi, S.; Iwasaki, I.; Shiraiwa, Y. Historical Perspective on Microalgal and Cyanobacterial Acclimation to Low- and Extremely High-CO2 Conditions. *Photosynthesis Research*. Springer 2003, pp 139–153. https://doi.org/10.1023/A:1025817616865

(68) Thomas, D. M.; Mechery, J.; Paulose, S. V. Carbon Dioxide Capture Strategies from Flue Gas Using Microalgae: A Review. *Environmental Science and Pollution Research* 2016, *23* (17), 16926–16940. https://doi.org/10.1007/s11356-016-7158-3

(69) Schnurr, P. J.; Allen, D. G. Factors Affecting Algae Biofilm Growth and Lipid Production: A Review. *Renewable and Sustainable Energy Reviews* 2015, *52*, 418–429. https://doi.org/10.1016/j.rser.2015.07.090

(70) Sekar, R.; Venugopalan, V. P.; Satpathy, K. K.; Nair, K. V. K.; Rao, V. N. R. Laboratory Studies on Adhesion of Microalgae to Hard Substrates. In *Asian Pacific Phycology in the 21st Century: Prospects and Challenges*; Springer Netherlands, 2004; pp 109–116. https://doi.org/10.1007/978-94-007-0944-7_14

(71) Di Pippo, F.; Ellwood, N. T. W.; Guzzon, A.; Siliato, L.; Micheletti, E.; De Philippis, R.; Albertano, P. B. Effect of Light and Temperature on Biomass, Photosynthesis and Capsular Polysaccharides in Cultured Phototrophic Biofilms. *J. Appl. Phycol.* 2012, *24* (2), 211–220. https://doi.org/10.1007/s10811-011-9669-0

(72) Kim, H. W.; Park, S.; Rittmann, B. E. Multi-Component Kinetics for the Growth of the Cyanobacterium Synechocystis Sp. PCC6803. *Environmental Engineering Research* 2015, *20* (4), 347–355. https://doi.org/10.4491/eer.2015.033

(73) Kesaano, M.; Sims, R. C. Algal Biofilm Based Technology for Wastewater Treatment. *Algal Res.* 2014, *5* (1), 231–240. https://doi.org/10.1016/j.algal.2014.02.003

(74) Liao, Q.; Li, L.; Chen, R.; Zhu, X. A Novel Photobioreactor Generating the Light/Dark Cycle to Improve Microalgae Cultivation. *Bioresour. Technol.* 2014, *161*, 186–191. https://doi.org/10.1016/j.biortech.2014.02.119

(75) Pospíšil, P. Production of Reactive Oxygen Species by Photosystem II as a Response to Light and Temperature Stress. *Front. Plant Sci.* 2016, *7* (DECEMBER2016). https://doi.org/10.3389/fpls.2016.01950

(76) Yamamoto, Y.; Aminaka, R.; Yoshioka, M.; Khatoon, M.; Komayama, K.; Takenaka, D.; Yamashita, A.; Nijo, N.; Inagawa, K.; Morita, N.; Sasaki, T.; Yamamoto, Y. Quality Control of

Photosystem II: Impact of Light and Heat Stresses. *Photosynthesis Research*. October 2008, pp 589–608. https://doi.org/10.1007/s11120-008-9372-4

(77) Schnurr, P. J.; Espie, G. S.; Allen, D. G. The Effect of Light Direction and Suspended Cell Concentrations on Algal Biofilm Growth Rates. *Appl. Microbiol. Biotechnol.* 2014, *98* (20), 8553–8562. https://doi.org/10.1007/s00253-014-5964-4

(78) Schnurr, P. *Understanding How Critical Growth Parameters Affect Algal Biofilm Growth and Internal Lipid Concentrations*; 2016.

841 **For Table of Contents Only**

842

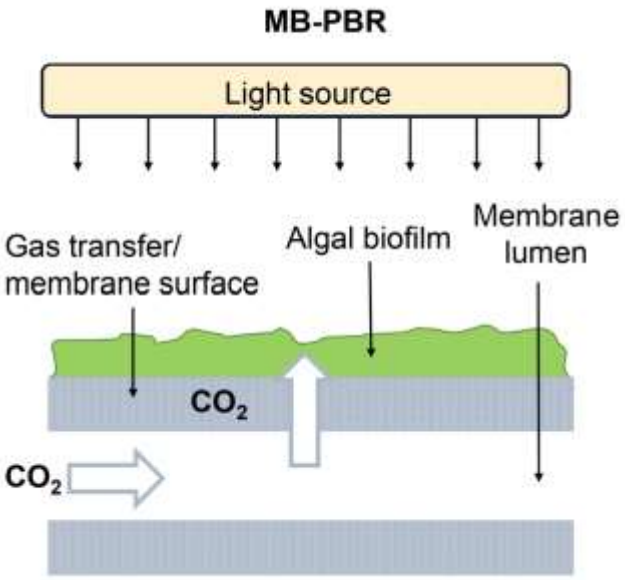

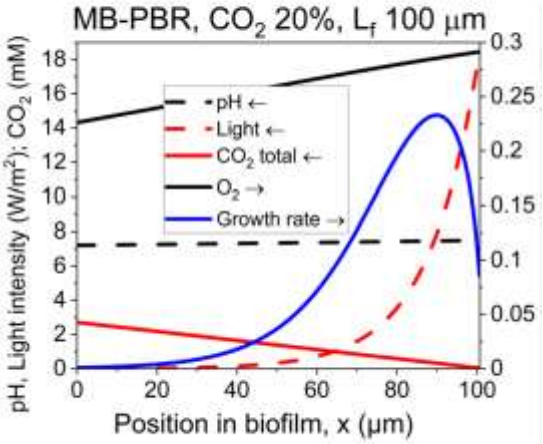

843

https://dspace.org/

Modeling biofilm growth on a CO2-supplying, membrane-based biofilm photobioreactor

Garcia-Perez, J. Saul; Garg, Meenu; Perez-Calleja, Patricia; Ontiveros-Valencia, Aura; Parra-Saldívar, Roberto ...

2026-04-10
American Chemical Society (ACS)
https://doi.org/10.1021/acsestengg.5c00994
Garcia-Perez JS, Garg M, Perez-Calleja P, et al., (2026) Modeling biofilm growth on a CO2-supplying, membrane-based biofilm photobioreactor. ACS ES&T Engineering, Volume 6, Issue 4, April 2026, pp. 1285-1296

Downloaded from a DSpace repository. https://dspace.org/